Transition Metal Chemistry
https://doi.org/10.1007/s11243-024-00621-7

Self-assembled heterometallic Cu(II)–Na(I) coordination polymer with salen-type Schiff base ligand: structural analysis, antimicrobial, DFT and molecular docking study

Sandeepta Saha[1,3] · Niladri Biswas[1,2] · Manas Chowdhury[1] · Kamal Kumar Ghosh[1] · Corrado Rizzoli[4] · Nayim Sepay[5] · Sharmila Chakraborty[6] · Mukut Chakraborty[1] · Chirantan Roy Choudhury[1]

Received: 17 May 2024 / Accepted: 12 November 2024
© The Author(s), under exclusive licence to Springer Nature Switzerland AG 2024

Abstract

In this work, one new heterometallic Cu(II)/Na(I) 3D coordination polymer $[CuNa(H\textit{hpmet})(H_2O)(OH)]_n$ (**1**) has been synthesized by using the Schiff base ligand namely, 2-[(*E*)-(2-hydroxyphenyl)methyleneamino]terephthalic acid [H_3*hpmet*], $Cu(NO_3)_2.6H_2O$ and NaOH. Complex **1** was characterized by elemental analysis, FT-IR, UV–Vis, NMR spectroscopic measurements along with and single-crystal X-ray diffraction study. The single-crystal X-ray diffraction (XRD) analysis reveals that in complex **1**, the copper (II) adopts a distorted square pyramidal geometry with the addition index parameter (τ) value 0.018 whereas Na(I) center possess tetrahedral geometry. Here, DFT study was carried out to give insight in HOMO–LUMO energy gap, MEP surface and topology analysis whereas Hirshfeld surface (HS) study further points toward packing interactions. In addition, complex **1** was investigated for its antibacterial efficacy toward Gram-positive and Gram-negative strains. Molecular docking assessed antibacterial potency of the complex **1** toward protein molecules.

Introduction

Utilization of non-covalent interaction leading to self-assembly of individual molecules is nowadays one of the major frontier research area [1–4]. Extensive study of self-assembly has already built a widespread development in the field of crystal engineering. In crystal engineering, premeditated synthesis of crystalline materials is possible, where the molecular self-assembly in the solid state can be interpreted from the understanding of molecular building blocks [5–8]. A designed synthesis of a predetermined assembly is an interesting area as it may be handy as a functional material, which can be used in supramolecular chemistry [9–14], liquid crystal engineering [15, 16], crystal engineering [17–19], molecular electronics [20, 21], host–guest chemistry [22–25], biotechnology [26, 27] etc.

But as a matter of fact, prediction of the self-assembled structure sometimes does not accomplish due to weak nature of directing forces. A minor change in the reaction condition or even a small modification of the ligand framework can be helpful to produce unprecedented self-assembled structures [28]. Typically, hydrogen bonding interactions are mainly responsible for designing the supramolecular motifs [29–31] but other weak forces such as π···π [32–36] and CH···π [37–39] interactions are also suitable.

The aggregation of soft metal centers leading to covalently bonded clusters is familiar [9–19], for example Ru- and Os-carbonyl [40–42] along with Au-clusters [43]. On the contrary, hard metal cations generally devoid of forming metal–metal bonds and usually need bridging ligands mainly carboxylate [44–46], oxide or hydroxide [47–50] for aggregation. Concerning the synthesis of multinuclear heterometallic complexes containing hard metal centers, two synthetic

✉ Chirantan Roy Choudhury
crchoudhury2000@yahoo.com

[1] Department of Chemistry, West Bengal State University, Barasat, Kolkata 700126, India

[2] Department of Biotechnology, Institute of Genetic Engineering, No. 30, Thakurhat Road, Badu, Madhyamgram, Kolkata, West Bengal 700128, India

[3] Sripur High School, Madhyamgram Bazar, Kolkata 700130, India

[4] Dipartimento S.C.V.S.A., University of Parma, Parco Area delleScienze 17/A, 43124 Parma, Italy

[5] Department of Chemistry, Lady Brabourne College, Kolkata 700017, India

[6] Department of Microbiology, Sammilani Mahavidhyalaya, Baghajatin, Kolkata 700094, India

Published online: 09 December 2024

strategies have been chosen. In the synthesis, polynucleating ligands exhibiting multi-inequivalent coordination sites can be used [51]. Otherwise, a ligand–metal complex which is coordinatively unsaturated can be used in the second step of the synthesis [52]. This second method has advantages over the former one, heterometallic complexes form with the systematic combination of the various metal ions used. In the presence of a hard center, the coordination chemistry of alkali metal ions has attracted interest so that it can build up molecular biomimetic systems capable of the selective transport of metal ions. Tridentate Schiff bases ligands, are the most used complexing agents for the alkali metal ions [51, 52]. In the recent years, bimetallic coordination compounds of 3*d*-n*s* metal ions have been the point of interest of several studies [53–56]. The simplest compartmental ligands are conceivably Salen-type Schiff bases, where their deprotonated units are enthralling side-off compartmental ligands with two dissimilar coordination spheres making it possible the formation of multi-metallic complexes [57–60]. The inner N_2O_2 compartment can accommodate a 3*d* metal ion, whereas the outer $O_2O'_2$ compartment is capable of binding with an additional metal ion to form 3*d*-*ns*, 3*d*-*np*, 3*d*-3*d* and 3*d*-4*f* homo- and heteronuclear complexes [53–67]. Recently, it is observed that square-planar Cu(II)–Na(I) complexes can be synthesized with Schiff bases obtained from the condensation of amines with hydroxylated aldehydes and saturating their residual coordination sites by simultaneous use of an auxiliary Na metal ions [68, 69].

Following this approach, the Schiff base ligand formed from the condensation of 2-amino terephthalic acid along with pyridine-2-carbaldehyde has been utilized by our group earlier [59, 63, 70].

With the endeavor for preparing new multinuclear heterometallic coordination polymers, the H_2*Pymat* Schiff base ligand was taken to incorporate an additional alcoholic donor group, as salicylaldehyde is taken in place of pyridine-2-carbaldehyde with a different synthetic approach. Generally, the Salen ligand (SL) is a distinct class of N/O-donor ligands (N_2O_2/N_2O_4-type) coordinated with M^{n+} ions via the N-atom of two azomethine group (–CH=N) accompanied with deprotonated phenolic O-atom. But, as we use a single amino group containing ligand, which generates a NO_2 type of ligand, the so-called compartment cannot be formed. Rather, due to the presence of carboxylato groups residing at para positions to each other enhances its ability to form supramolecular motifs, which is clearly evident from our previous works [59, 63, 70], The Schiff base, 2-[(*E*)-(2-hydroxyphenyl)methyleneamino]terephthalic acid (H_3*hpmet*, Scheme 1), was prepared by the condensation reaction of 2-aminoterephthalic acid and salicylaldehyde.

A new 3D coordination polymer [CuNa(H*hpmet*)$(H_2O)(OH)]_n$ (**1**) has been prepared (Scheme 2) and characterized by elemental analysis, FT-IR, UV–Vis, NMR spectroscopic measurements along with and single-crystal X-ray diffraction study. Here, DFT study was carried out to find out HOMO–LUMO energy gap, MEP surface and topology whereas Hirshfeld surface (HS) study further analyzed the packing interactions. In addition, complex **1** was investigated for its antibacterial efficacy toward Gram-positive and Gram-negative strains and molecular docking study was carried out to find out the antibacterial potency of the complex **1** toward protein molecules.

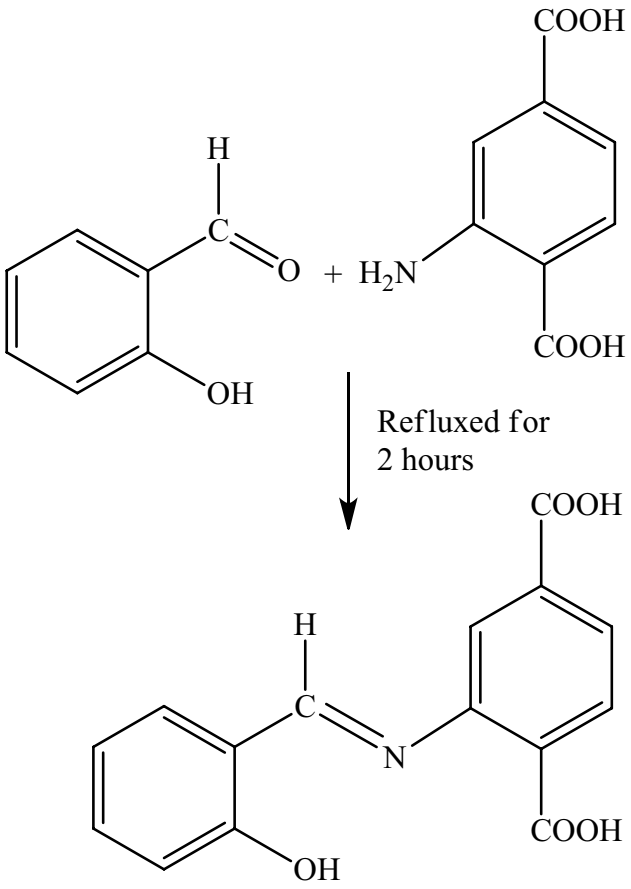

Scheme 1 Synthetic scheme of 2-[(*E*)-(2-hydroxyphenyl)methyleneamino]terephthalic acid [H_3*hpmet*]

Experimental section

Materials

$Cu(NO_3)_2{\cdot}3H_2O$ and NaOH were purchased from E Merck, India and DMSO was obtained from SRL. 2-Aminoterephthalic acid and salicylaldehyde were purchased from Sigma-Aldrich. All solvents and reagents were of reagent grade and were used as received without further purification.

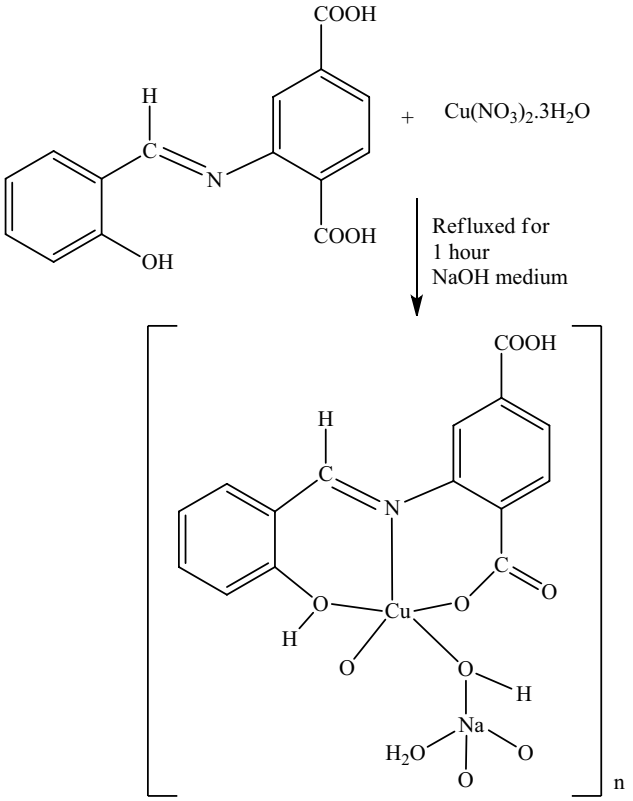

Scheme 2 Synthesis of Complex **1**

Physical measurements

The infrared spectrum of complex **1** was recorded on a Perkin–Elmer SPECTRUM 2 FT-IR spectrophotometer with KBr disks (4000–400 cm^{-1}). An electronic spectrum of complex **1** was recorded at 300 K on a Perkin-Elmer Lambda-35 UV–Vis spectrophotometer in DMSO medium. Elemental analyses (C, H, N) were carried out using a Perkin–Elmer 2400 II elemental analyzer.

^{1}H and ^{13}C NMR spectra of ligand (HL) were recorded in a Bruker 400 MHz instrument using TMS as an internal standard. EDX was performed by using a W filament on the OXFORD XMX N model. High-resolution SEM images were analyzed with the JEOL model JSM-6390LV.

Synthesis

Synthesis of the ligand [H_3*hpmet*]

2-Aminoterephthalic acid (5 mmol, 0.906 g) and salicylaldehyde (5 mmol, 0.610 g) were taken in 25 mL methanol. The yellow colored reaction mixture was heated under reflux condition for 2 h. Within 30 min of heating, the mixture turned deep orange. After reflux, the orange reaction mixture was cooled to room temperature. ^{1}H NMR (DMSO-d_6, 400 MHz, 25 °C), d (ppm): 3.43 (1H, *s*), 7.52 (1H, *d*), 7.48 (1H, *t*), 6.91 (1H, *t*), 7.50 (1H, *d*), 7.83 (1H, *s*), 7.28 (1H, *s*), 10.25 (1H, *s*), 7.50 (1H, *d*), 7.02 (1H, *d*), 9.85 (1H, *s*). (Figs. S3A and S3B, Supplementary information).

^{13}C NMR ($CDCl_3$, ppm): 161.15 (C1), 151.60 (C2), 115.22 (C3), 113.14 (C4), 136.90 (C5), 135.66 (C6), 169.51 (C7), 192.37 (C8), 122.72 (C9), 167.56 (C10), 117.68 (C11), 131.88 (C12), 118.00 (C13), 129.82 (C14), 119.97 (C15). (Fig. S4A and B, Supplementary information).

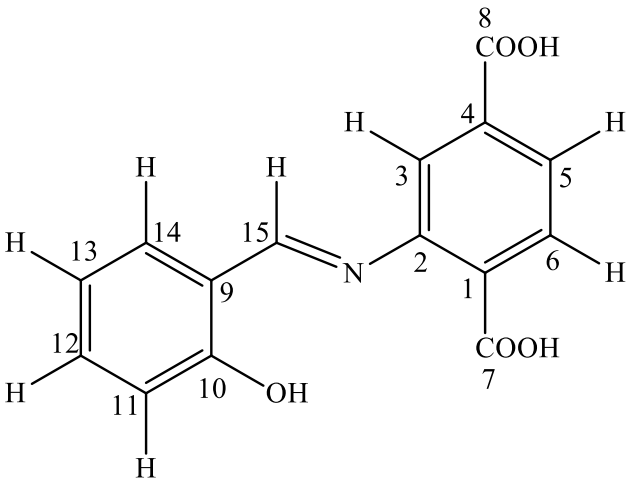

Schematic diagram of ligand mentioning the number of carbon atoms.

Synthesis of the complex [CuNa(H*hpmet*)(H_2O)(OH)]$_n$ (1)

$Cu(NO_3)_2{\cdot}3H_2O$ (0.241 g, 1 mmol) and the ligand H_3*hpmet* were dissolved in 20 mL of methanol. The reaction mixture was refluxed for 1 h resulting in a green precipitate along with a green colored solution, which was further treated with 2 mmol of NaOH (0.4 g) dissolved in a few drops of water and stirred for 2 h at room temperature. After that, the mixture was filtered and the filtrate was left to evaporate. Blue block-shaped single crystals suitable for single-crystal X-ray diffraction analysis were obtained after 2 weeks.

Yield: 0.293 g (71%). Anal. Calc (%) for $C_{15}H_{12}Cu_1N_1Na_1O_7$: C, 44.47; H, 2.96; N, 3.46. Found: C, 44.72; H, 2.93; N, 3.41%.

Fourier transform infrared (FT-IR) (KBr, cm^{-1}): 3436(b), 3018(s), 2530(b), 1608(s), 1576(m), 1504(s), 1467(s), 1437(m), 1369(s), 1311(s), 1214(m), 1024(m), 850(s), 819(m), 770(s), 756(s), 690(s), 527(w), 510(w), 489(m), 464(m).

X-ray crystallography

A single crystal of complex **1** was mounted on a Bruker APEX-II CCD diffractometer equipped with graphite

monochromatized Mo Kα ($\lambda = 0.71069$ Å) fine-focus sealed tube. Intensity data were collected at 292(2) using ω scans. Crystal data were collected using APEX2. Data refinement and reduction were performed using SAINT (Bruker 2008) [71] software. Multi-scan absorption corrections were applied empirically to the intensity values using SADABS [71]. The structures were solved by direct methods using the program SIR97 [72] (Altomare et al. 1999), and refined with full-matrix least-squares based on F^2 using program SHELXL-2019/3 (Sheldrick 2015) [73]. All non-hydrogen atoms were refined anisotropically. H atoms attached to carbon atoms were positioned geometrically (C–H = 0.93 Å) and refined in the riding-model approximation, with C−H = 0.82–0.93 Å and with $U_{iso}(H) = 1.2U_{eqv}(C)$. A rotating model was used for the O5 and O6 hydroxyl groups. The water molecule is disordered over two orientations with refined site occupancy factors of 0.74(3):0.26(3). The displacement ellipsoids of the disordered oxygen atom were restrained to be equal and nearly isotropic. The Na1−O_{water} distances were also restrained to be similar. The water H atoms were placed in chemically sensible positions on the basis of plausible hydrogen bonds [O–H = 0.86(1) Å, H···H = 1.36(2) Å] and allowed to ride on the oxygen atom with $U_{iso}(H) = 1.5U_{eqv}(O)$. The molecular graphics and crystallographic illustrations complex were prepared using CAMERON [74], PLATON [75], DIAMOND [76], POV-RAY [77] and OLEX2 [78] programs. All the relevant crystallographic data and structure refinement parameters complex **1** are summarized in Table 1.

Table 1 Crystallographic data and structural refinement of complex **1**

	1
Empirical formula	$C_{15}H_{12}Cu_1N_1Na_1O_7$
Formula weight (g mol^{-1})	404.79
Temperature	292(2)
Crystal system	Monoclinic
Space group	*P21/n*
a (Å)	9.6485(6)
b (Å)	7.4432(5)
c (Å)	21.7954(13)
β (deg)	90.9630(9)
V ($Å^3$)	1565.03(17)
Z	4
d_{calc} (g cm^{-3})	1.718
μ (mm^{-1})	1.463
F (000)	820
Crystal size (mm^3)	0.12 × 0.14 × 0.16
θ range (deg)	1.87 – 25.25
Measured reflections	14957
Independent reflections	2837
R(int)	0.029
Goodness-of-fit on F^2	1.059
Final *R* indices[$I > 2\sigma(I)$]	$R_1{}^a = 0.0395$, $wR_2{}^b = 0.1116$
R indices (all data)	$R_1{}^a = 0.0458$, $wR_2{}^b = 0.1170$
$\Delta\rho_{min}$ and $\Delta\rho_{max}$(e $Å^{-3}$)	−0.67 and 0.57

[a] $R_1 = \Sigma||F_o|-|F_c||/\Sigma|F_o|$, [b] $wR_2 = \{\Sigma[w(F_o{}^2-F_c{}^2)^2]/\Sigma[w(F_o{}^2)^2]\}^{0.5}$

Hirshfeld surface

There are points on the Hirshfeld surface which indicate half or more of the electron density available from the atoms of this molecule [79, 80].

Hirshfeld surface plots and 2D fingerprint plots [79–83] were computed using CRYSTAL EXPLORER 3.1 [80]. In this study, the Hirshfeld surface has been mapped over normalized contact distances (d_{norm}). In terms of *de* versus d_i, we presented the shape index and decomposed fingerprint plot. The d_{norm}, expressed as $\left(d_i - r_i^{vdw}\right)/r_i^{vdw} + \left(d_e - r_e^{vdw}\right)/r_e^{vdw}$; where r_i^{vdw} and r_e^{vdw} are the *van der Waals* radii of the atoms, indicates the regions having the ability to intermolecular interactions. In a crystal structure, a supramolecular structure results from the extended form of close three-dimensional contacts. The surface map was calculated within Crystal Explorer via TONTO using the B3LYP/6–311G(d,p) ± 0.03 a.u. method.

DFT study

Using hybrid functional B3LYP with mixed basis sets 6-31++G(d,p)/LANL2DZ, DFT calculations were carried out on **1** (in isolated form). Gaussian 09 and the molecular visualization software Gauss-View 5 were utilized for DFT [84, 85]. In the framework of DFT, the spin-unrestricted scheme was employed because the complex has odd electrons (one unpaired electron). The X-ray refinement structure was used as the starting geometry for geometry optimization calculations. To understand the reactive nature of the present complex, frontier molecular orbitals (FMOs) were also presented. The same level of theory was applied to the MEP calculations.

Topology analysis

To analyze crystal topology, the Topos Pro software package was applied along with the TTD collection of periodic network topologies [86] The RCSR three-letter codes identifies complex network topologies. The Topos NDn nomenclature is used for network types not covered by the RCSR designation methodology [87]. The *N* represents the sequence of coordination numbers for all non-equivalent nodes in the net; the *D* represents its periodicity (*M*, *C*, *L*, and *T* for 0-, 1-, 2-, and 3-periodic nets, respectively); and the n represents the ordinal number of this net among all non-isomorphic nets [88].

Table 2 Mean zone diameter for compound **1**

	Mean zone diameter (mm)[a]			
	E. *coli*	K. *aerogenes*	B. *subtilis*	S. *aureus*
Complex 1	19 ± 0.4	10 ± 0.1	14 ± 0.3	18 ± 0.2
DMSO	–	–	–	–

[Each value represents a mean ± standard deviation (SD) of three measurements. [a]The zone diameter have been calculated (mm).]

Antimicrobial assay

Nutrient agar plates were prepared and sterilized. Bacterial cells were grown overnight in liquid nutrient agar medium. On the next day 0.1 ml of the overnight bacterial culture was put on the surface of agar and spread evenly with the help of a spreader. Wells were made diameter of the bore adjusted so as to contain 50 µl of sample) with curk borers and agar pieces safely discarded. 50 µl of each sample was into each well poured with the help of a micropipette. The samples were diluted to desired concentrations of l mg/ml and 5 mg/ml.

Plates were kept at 4 °C to initiate uniform diffusion. Plates were incubated at 37 °C overnight without inverting. The next day zones were observed and the diameters recorded in Table 2.

Organisms used in this experiment are two kinds of bacteria.

Gram Positive—(a) Bacillus subtilis, (b) Staphylococcus aureus.

Gram negative—(a) Escherichia coli, (b) Klebsiella aerogenes.

The minimal inhibitory concentration of complex 1 against bacteria

The minimum inhibitory concentration (MIC) to kill bacterial population (99%) against the bacterial strain with complex **1** was determined using standard method. Overnight bacterial culture of Gram + Ve and Gram – Ve bacteria were used for the experiment.

One tube is considered as positive control (with inoculum) and another is negative control (no inoculum). Inoculum of Escherichia coli was added to the 2X NB prior to distribution of the broth in each test tube. After distribution contents of the each tube mixed properly and were incubated at 37 °C for 24 h. Results were recorded the next day and are represented in Table 3. From the results, MIC of the bacteria against complex **1** was calculated in µg/ml.

Table 3 Minimum inhibitory concentration (MIC) (µg/ml) values of complex **1** against microbes

Sample	MIC (µg/ml)			
	Gram – ve bacteria		Gram + ve bacteria	
	E. *coli*	K. *aerogenes*	B. *subtilis*	S. *aureus*
Complex 1	11.25	11.25	11.25	11.25

Molecular docking study

The energy-minimized structure of the complex was used for the molecular docking. The process involved creating pdbqt files and assigning partial charges to both molecules and proteins was performed using AutoDock Tools (ADT). These structures were then used in docking simulations with AutoDock 4.2, following the standard docking protocol outlined in the AutoDock 4.2 manual. We established sizable 3D grids with dimensions of 40 × 40 × 40 Å (*X*, *Y*, *Z*) and a grid spacing of 1 Å to encompass all binding sites, customizing the grid box coordinates based on the protein. The docking calculations were carried out using AutoDock 4.2 with the Lamarckian genetic algorithm, and the visualization of the docking results was achieved using Pymol with Schrödinger Release 2023.

Results and discussion

Syntheses

We mostly intended to synthesize a Na(I)/Cu(II) heterometallic coordination complex using a tridentate ONO donor Schiff base ligand. Our purpose was to explore the structural variations acquired by the ligand and the complex in presence of the carboxylate groups of the ligand.

Generally, Salen or Valen type of Schiff Base ligands upon reaction with copper salt form square pyramidal or square-planar complexes [89, 90]. When Na(I) is incorporated in the structure, the geometry of Cu(II) changes from square pyramidal to square planar and the hard metal centers acquire an octahedral geometry [91–93]. It is worth mentioning here that being a non-compartmental ligand, usually in the presence of a sodium salt, salen-type ligands form trinuclear Cu(II)–Na(I)–Cu(II) systems [91, 93]. But, interestingly in this case due to presence of the carboxylic groups together with a bridging hydroxyl group we obtain a 3D structure, where the Cu(II) ion acquires the square pyramidal and Na(I) the tetrahedral geometry. Unexpectedly, the solvent molecule does not play any part in the self-assembly apart from barely satisfying a secondary valency of the Na(I) ion.

Infrared spectral study

Infrared spectrum of complex **1** was recorded in the region 4000–400 cm^{-1} (Fig. S1). Complex **1** showed (C=N) stretching frequency at 1608 cm^{-1} due to the presence of the deprotonated coordinated ligand [94]. For complex **1**, a broad peak was observed at 3436 cm^{-1} which stands for the ν(O–H). Another two peaks appeared at 527 and 464 cm^{-1} which can be assigned to (M–O) and (M–N) stretching frequency, respectively [95]. The significant vibrations of the benzene ring skeleton in **1** was observed in the region 1437–1467 cm^{-1} [96]. Complex 1 displayed ν_{assym} (COO^{-}) peak at 1576 cm^{-1} and ν_{sym} (COO^{-}) peak at 1332 cm^{-1}. The difference $\Delta\nu = \nu_{assym} - \nu_{sym}$ is 244 cm^{-1}, which clearly indicate the monodentate nature of the bridging acetate [97–100]. Infrared stretching frequency near 3018 cm^{-1} was observed for the C–H group [97].

Electronic spectral study

The UV–Vis absorption spectrum of complex **1** in DMSO was recorded in the region 200–800 nm (Fig. S2). The spectrum showed band at 270 nm corresponding to intraligand $\pi \rightarrow \pi^*$ transition of the coordinated imines [95]. Complex **1** displayed a shoulder band at 382 nm and 372 nm which can be attributed to $n \rightarrow \pi^*$ transitions [101, 102]. The low-intensity band observed at 662 nm can be attributed to $d \rightarrow d$ transition [101, 102].

Description of crystal structure of complex 1

Single-crystal X-ray analysis reveals that complex **1** crystallizes in the monoclinic space group *P*21/*n*. An ORTEP view of complex **1** with atom numbering scheme is shown in Fig. 1.

The hydrogen atom of the oxygen at the apical position of the pyramid about the Cu atom was evident in the difference Fourier map, while the H atoms of the phenol ring and disordered water molecule were not; it is therefore we assume that the O6 atom is in fact an hydroxy group and that the O5 phenolic oxygen is protonated. Moreover, all H atoms of the disordered water molecule were calculated on the basis of plausible H-contacts.

Crystallographic data and structural refinement of complex **1** and selected bond lengths and bond angles are summarized in Table T2 (Supplementary information).

The fundamental building unit of complex **1** contains one copper(II) metal ion, one ligand moiety $hpmet^{2-}$, one hydroxide group, a sodium(I) atom and a terminal water molecule. The copper center adopts a distorted square pyramidal geometry with two different ligands and the hydroxide group in which the copper(II) ion is located 0.2437(4)Å above the N_2O_2 basal plane (r.m.s. deviation = 0.0206 Å). In this case,

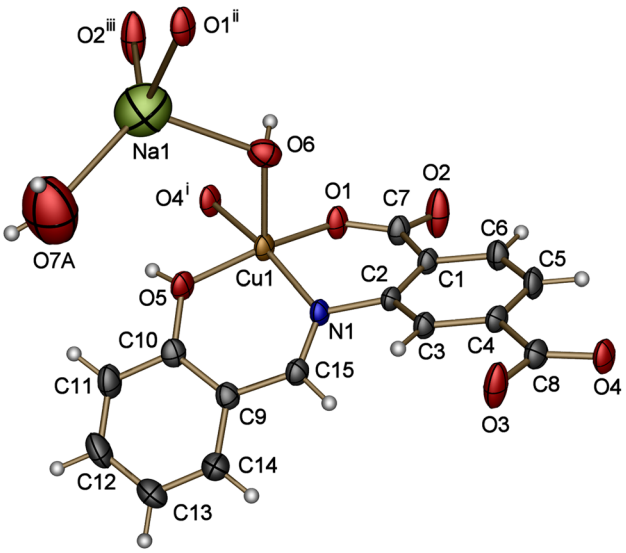

Fig. 1 The asymmetric unit of **1** with displacement elllipsoids drawn at the 50% probability level. Only the *A* component of the disordered water molecule is shown. Symmetry codes: (i) 1 + x, y, z; (ii) x, − 1 + y, z; (iii) 1 − x, − y, − z

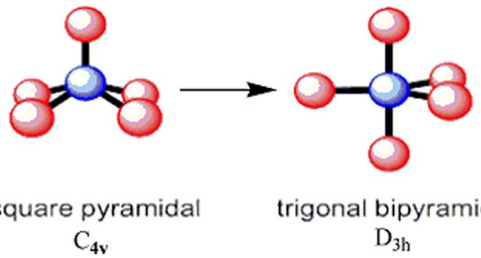

Scheme 3 Distortion in SQP geometry

it is worth mentioning that, for penta-coordinated Cu(II) complexes, geometry can exist in three different forms. For instance square pyramid (SQP), trigonal bipyramid (TBP) and intermediate between SQP and TBP. The SQP geometry can easily be changed into TBP geometry by simple bonds rotation, as the $d_x^2 - _y^2$ electronic ground state is expected in SQP, whereas the d_z^2 electronic ground state is anticipated in TBP (Scheme 3).

In real systems, ideal geometries are hardly ever achieved. The electronic effect (electron donating or withdrawing) of substituents could be an imperative factor that may tune ligand field strength and selectively favor $d_x^2 - _y^2$or d_z^2 ground state in Cu(II) center. The copper(II) ion in complex **1** deviate slightly from the ideal SQP geometry with Addition parameter [103] $\tau = 0.018$. The ligands are bonded to the copper atom through N1, O1, O5, $O4^i$ and O6. The hydroxo oxygen atom (O6) is situated at the apical position of the pyramid and the rest of the atoms (N1, O1, O5 and $O4^i$;

i = 1 + *x*, *y*, *z*) form the basal plane. N1 is the imine nitrogen atom and O1 and $O4^{i}$ are oxygen atoms from the carboxylate group ortho to the imino group. Among these set of atoms N1, O1 and O5 belong to same ligand moiety, whereas $O4^{i}$ comes from a symmetry-related ligand and, due to presence of two carboxylate groups placed *para* to each other, the ligand thus acts as a bridging ligand. Within the carboxylate groups, it should be noted that the C7–O2 and C8–O4 bonds (mean value 1.239(8) Å) show a remarkable double bond character, indicating that the negative charges should be localized on the O1 and O3 oxygen atoms (the mean value of the C7–O1 and C7–O3 bond lengths is 1.289(10) Å). The Cu–O1 (1.922(2) Å) and Cu–N1 (1.959(2) Å) bond lengths compare well with those reported in the literature for ligands featuring a μ-carboxyphenylsalicylideniminato moiety (mean values: 1.932 and 1.968 Å, respectively, calculated over 34 entries in the CSD database). The mean value of the Cu–O bond lengths involving the neutrally charged hydroxyl (O5) and carboxylate ($O4^{i}$) atoms is 2.00(7) Å.

The angles subtended the Cu atom ranges from 84.00(8)° to 165.77(10)°. The two six-membered chelate rings adopt an approximate twist-boat conformation, with puckering parameters $Q = 0.390(2)$ Å, $\theta 2 = 65.7(4)°$, $\varphi 2 = -34.2(4)°$ for Cu1/O1/C7/C1/C2/N1 and $Q = 0.412(2)$ Å, $\theta = 59.6(4)°$, $\varphi = 21.4(4)°$ for Cu1/O5/C10/C9/C15/N1.

The coordination geometry around Na(I) can be described as a tetrahedral geometry as it is evident from the bond angles around the sodium atom shown in Table 2. The coordination sites are being defined by four oxygen atoms, namely O1, O2, O6 and O7. O1 and O2 are carboxylato oxygen atoms belonging to different ligands and O6 is the hydroxo oxygen atom a μ_2-bridging the copper and sodium atoms. O7 comes from the terminal water molecule. The ligand displays two types of coordination mode, that is μ_3-bridging with one carboxylate group in a μ_2-η^2:η^1 chelating bridging mode connecting two sodium(I) and a copper(II) atom or in a monodentate mode. The separation of two Cu(II) ions bridged by the same ligand is 9.6485(7) Å. Such a μ_2-η^2:η^1 chelating bridging mode (*syn–syn* with respect to sodium atom and *syn-anti* with respect to sodium and copper atom) of the carboxylate group leads to the formation of a binuclear unit with a Na1···Na1 distance of 4.112(6) Å. As a consequence, the adjacent binuclear units are connected alternatively via the hydroxide group to afford a cyclic tetranuclear motif. These tetranuclear motifs are further extended to form a 1D chain along the *c* axis and the adjacent 1D strand are further connected via Cu1 atom to form the 2D sheet (Fig. 2a). A close insight into the structure reveals that two 2D sheets are arranged to form a layered structure which produces a small void in the cluster (Fig. 2b). The water molecule along with the phenoxo and hydroxo group present in the ligand shows strong intra- and intermolecular hydrogen bond with the carboxylate groups. The hydrogen bonds may be categorized as both classical O−H···O type and nonclassical C−H···O type along with π−π interactions (Fig. 2c) with a separation of 3.7538(12) Å between the aromatic rings. Details of the pattern of hydrogen bonds are given in Table S1.

SEM–EDX analysis

The SEM micrograph of the Schiff base and the complex **1** (Figs. S5 and S6, respectively, Supplementary information) explored the surface morphology. The SEM image of the Schiff base shows ice-like morphology, similar to what has been reported in the literature [61, 62]. The surface of the complex **1** shows flakes like overlapping sheets spread throughout the micrographs establishing the sample's homogeneity. Elemental composition of the Schiff base and the metal complex are explored by using EDX profile (Fig. S7 for Schiff base and Fig. S8 for complex **1**) [61, 62, 64]. In the EDX profile, the Schiff base (Fig. S7) shows the presence of carbon (C), oxygen (O), nitrogen (N) whereas the complex **1** comprises of carbon (C), oxygen (O), nitrogen (N), copper (Cu) and sodium (Na) metal ions (Fig. S8) confirming the formation of metal–ligand complex. The EDX profile confirms the interaction among Cu(II), Na(I) and Schiff base ligand [61, 62, 64].

Hirshfeld surface (HS) analysis

In the graphic below (Fig. 3), two adjacent interacting molecules are shown in their relative position over d_{norm}. The d_{norm} HS surface uses color coding, which is blue, white, and red. These colors indicate how far apart two neighboring atoms are from each other based on their respective van der Waals radii. Therefore, in the case of red spots, van der Waals radii can be approximated with significant accuracy for atoms involved in non-covalent interactions [79, 80].

Seventeen bright red spots having different size were found over d_{norm} surface of the complex (Fig. 3a) which may form H-bonding interactions with adjacent molecular fragments. The blue regions on the same surface also show the available surface for other type of strong non-covalent interactions. The three-dimensional d_i surface of the 2D coordination polymer is demonstrated in Fig. 3b. In the shape-index surface of the complex (Fig. 3c), there are triangle shaped red and blue sports placed side-by-side. It indicates that these regions are capable of the formation of π–π stacking interactions between two adjacent molecules. On the HS, the curvedness provides the understanding of the coordination number in the crystal. The curvedness of HS (Fig. 3d) is very sharp in the Na^+ ion containing regions of the complex whereas it is less prominent over aromatic regions. The surface indicates that the Na^+ ion may form more non-covalent interactions with other neighboring

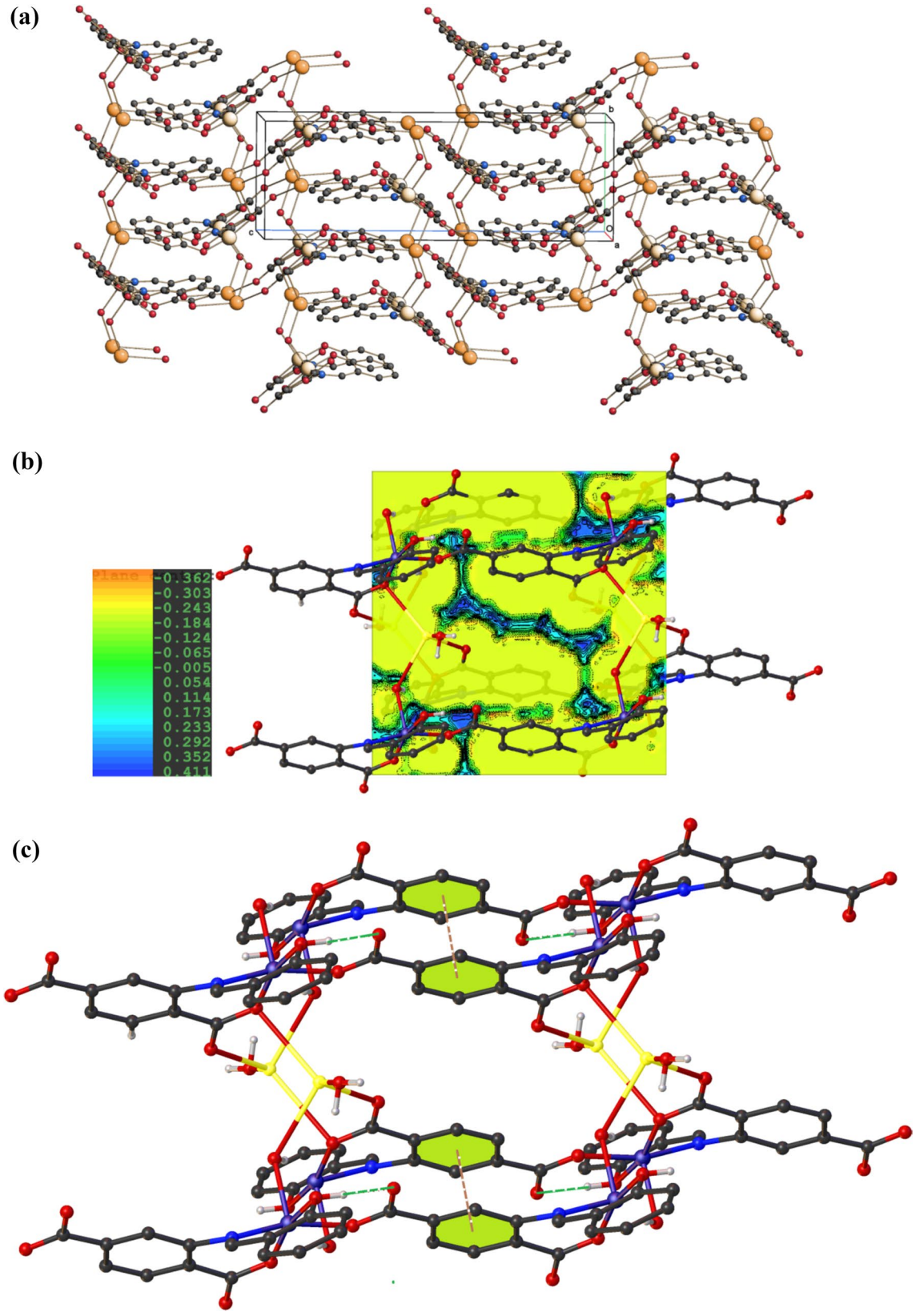

Fig. 2 **a** Packing diagram of **1** approximately viewed down the *a* axis. Hydrogen atoms and the B component of the disordered water molecule are omitted for clarity. **b** Voids in the cluster of **1**. **c** The hydrogen bonds (green dotted line) along with $\pi-\pi$ (brown dotted line) interactions in **1**

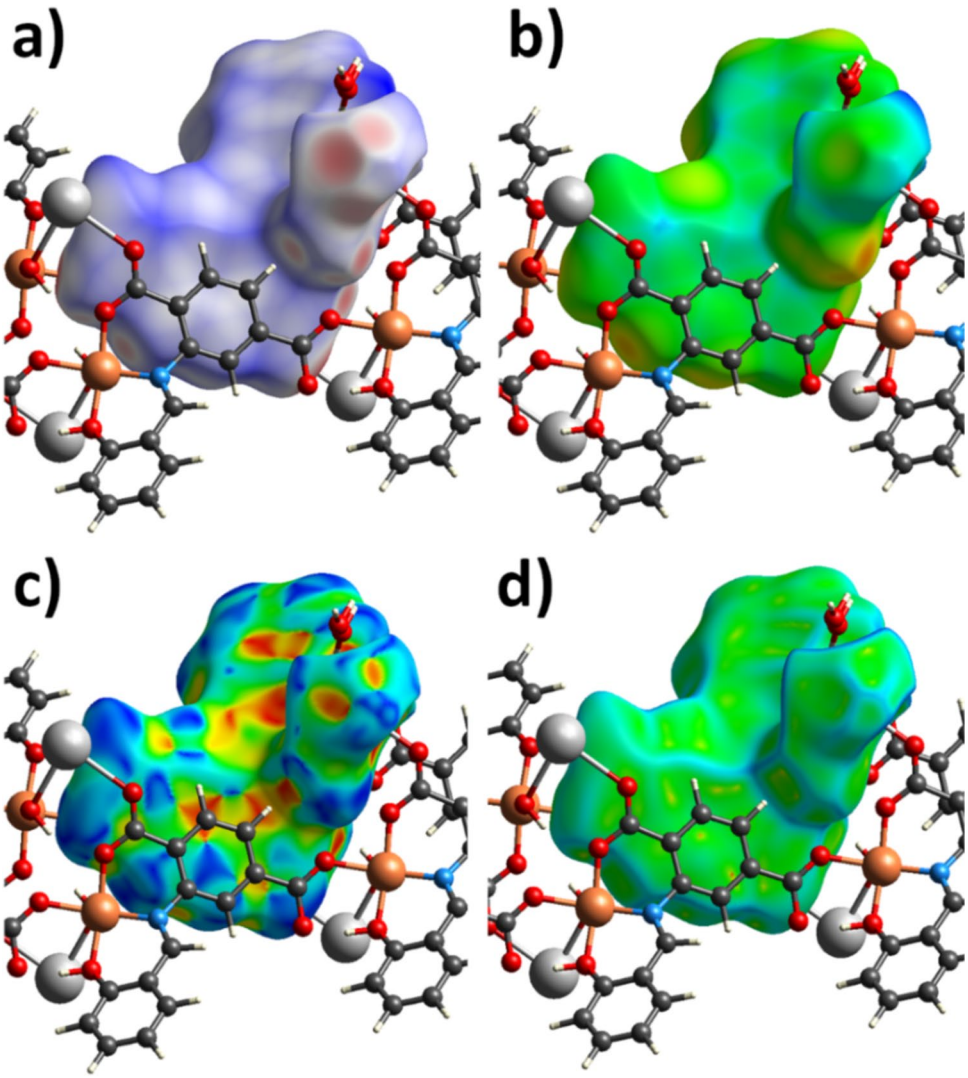

Fig. 3 **a** d_{norm}, **b** d_i, **c** shape-index and **d** curvedness Hirshfeld surface of an asymmetric unit of complex **1**

atoms. All types of non-covalent interactions present in the molecules can be identified and measured quantitatively with the help of d_i *vs* d_e fingerprint plots.

The fingerprint plot of d_e against d_i shows strong intermolecular non-covalent interactions present in the network of the molecules in the crystal (Fig. 4a). It is interesting to note that the O···H interactions are 29.6% of the total interaction which is the highest. Therefore, strong O···H interactions ($d_e = d_i < 1$ Å) may be the driving force and the key component for the crystal formation which is evident from the two sharp spikes in Fig. 4b. After this, C···H contacts are most important in the crystal formation which is 19% of the all non-covalent interactions (Fig. 4c). The extent of *van der Waals* H···H contacts in the crystal network is very close to the C···H contacts totaling 18.9% of the total contacts with $d_e + d_i = 1.9$ Å (Fig. 4d). The Na···O interactions are enough strong since $d_e = d_i = 1.4$ Å and 9.9% of the total interaction in the crystal (Fig. 4e). However, the C···C interaction in the crystal is strong and concentrated in a very tight region depicted by the cyan color patch in Fig. 4f. It was found to be 6.7% of the all type of contacts. Therefore, the HS analysis shows that the asymmetric unit of the polymer is mainly amphiphilic which will make it available to interact with diverse types of molecules.

Density functional theory

To understand the chemical reactivity of a compound, density functional theory can be used [81, 82]. The filled molecular orbital having highest energy (HOMO) is the most important orbital because it is involved when the molecule reacts with another molecule through electron donation. However, the molecule can behave as electrophile if can accept electron from an adjacent molecule at the lowest energy unoccupied molecular orbital (LUMO). Therefore, a small gap between HOMO and LUMO actually indicates high reactivity of the complex. In **1**, the energy gap is only 2.81 eV (Fig. 5). It is interesting to notice the presence of

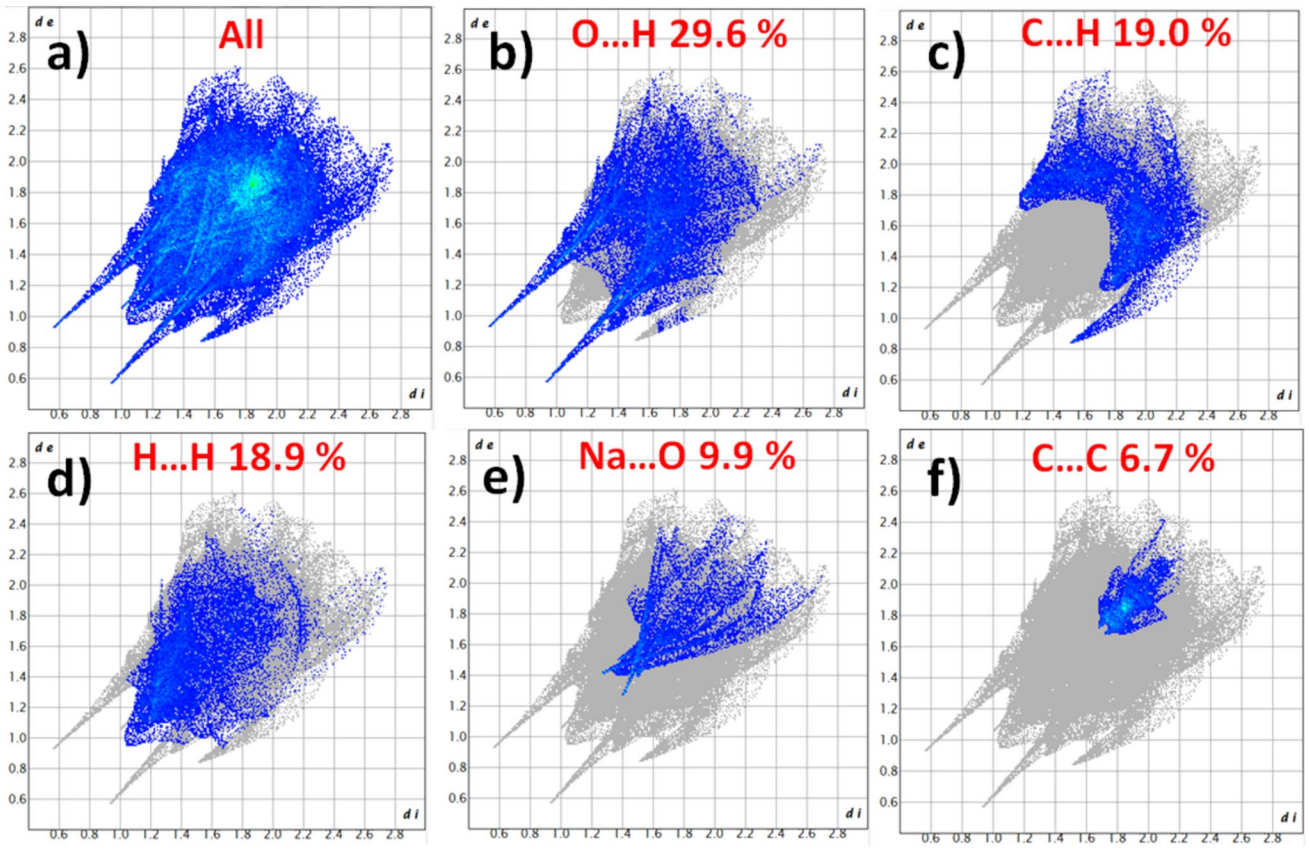

Fig. 4 The d_i versus d_e fingerprint plots **a** all, **b** O···H, **c** C···H, **d** H···H, **e** Na···O and **f** C···C interactions present in the network of the crystal

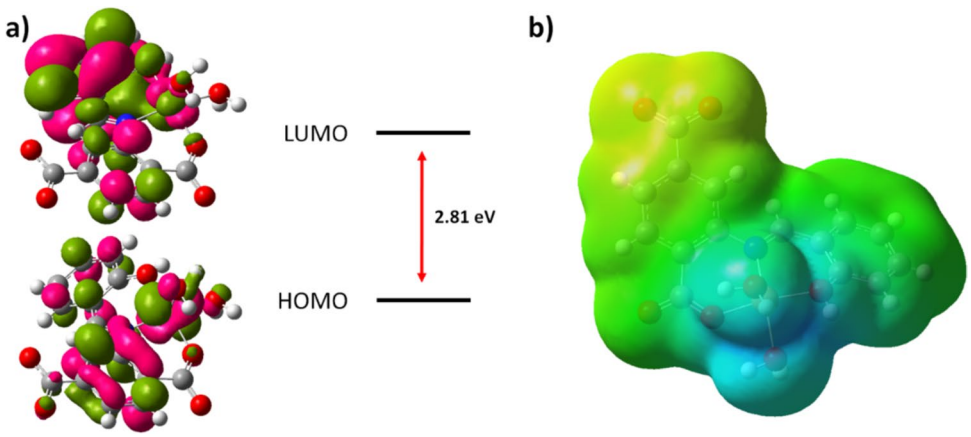

Fig. 5 **a** HOMO–LUMO energy gap and **b** molecular electrostatic map (MEP) of complex **1**

electron density over the metal ion in both HOMO and LUMO. It indicates that, in chemical reactivity, the complex have active participation through the metal ion. The HOMO is distributed almost all over the molecule whereas the LUMO concentrated more over the 2-aminobenzoic acid part.

A molecular electrostatic potential (MEP) map has also been calculated to get more structural information. The color coding of the MEP indicates the electron density around the molecule. The red and yellow regions on the surface demonstrate more and moderate electron density, respectively, and the blue region shows the electron-deficient atoms. In this case, the yellow region was found to be on nitro and carboxylic acid groups which indicate they can form the H-bond as H-bond acceptor. In contrast, the blue regions are associated with the phenolic OH and water OH groups, confirming their role as hydrogen bond donors. This suggests that the molecule can effectively

engage in hydrogen bonding interactions with other molecules. Moreover, this finding is further supported by the form Hirshfeld surface analysis, which reveals that 29.6% of total interactions are indeed hydrogen bonds within the crystal structure. The expansive green areas of the molecule underscore its significant π-interaction capability in the aromatic region. This conclusion is reinforced by the HS results, showing 19% C…H interactions, 18.9% H…H interactions, and 6.7% C…C interactions. Overall, the molecule demonstrates clear amphiphilic properties, enabling it to interact with a diverse range of other molecules.

Topology

Generally, coordination polymers consist of rigid ligands rather than a predictable topology resulting from the formation of strategic coordination complexes. Depending on metal ion geometry, ligand conformational flexibility, and functional groups, these can vary creating a molecular network with unpredictable topology and properties. In this complex, due to the involvement of the Na^+ ion in the coordination with an acid group, the complex has very complex crystal structure.

Using the centers of mass of ligands and/or groups on these molecules, we simplified the structure to identify the topology. In this study, a zig-zag-like 1D chain topology is found in the network that resembles the polymeric network of the Cu and Na complexes (Fig. 6). Considering all the covalent and ionic compounds, the coordination polymeric compound in the solid state have an unknown topology 3^6, 4-c net]. The molecules have created a valence-bonded MOFs like topology with symbol 3, 3, 4L34.

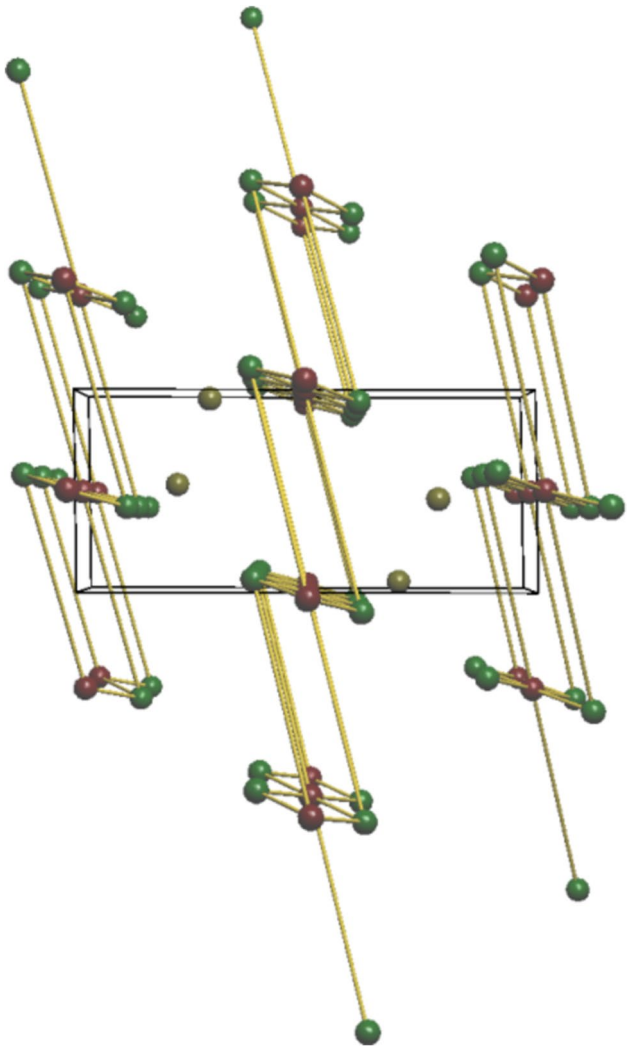

Fig. 6 Topology of the complex **1** in the solid state

Antimicrobial study

Zone diameter calculation

The zone diameter of the copper complex **1** was analyzed against two Gram positive and two Gram-negative bacteria.

Gram Positive—Bacillus subtilis and Staphylococcus aureus.

Gram negative—Escherichia coli and Klebsiella aerogenes.

The mean values of zone diameters are recorded in Table 2.

The compound showed very good activity against the chosen microbes and the order of reactivity was E. *coli* > S. *aureus* > B. *subtilis* > K. *aerogenes*.

The antimicrobial property showed by the complex is more or less close to the standard drugs (Given in Table 2).

MIC calculation

The complex **1** showed good antimicrobial activity against both Gram + ve and Gram –ve bacteria. Table 3 summarizes the MIC values of complex **1**. The complex had a value 11.25 µg/ml against all the selected microbes.

From the zone of inhibition and MIC values (11.25 µg/ml), it is evident that complex 1 showed very similar activity against a broad range of bacteria. It might be due to the fact that toxicity is increased due to the chelation of the Schiff base ligand with copper and the same can be explained by Tweedy's chelation theory [104, 105]. The polarity of the metal center is now lower due to coordination with ligands which ultimately increases the lipophilicity of the central metal atom. This fact in generally favors permeation through the lipid layer of microorganism leading to destroy them more efficiently [104]. The

antimicrobial activity of the complex **1** was more or less comparable with reported Cu(II) complexes [105–108].

Molecular docking study

Utilizing the optimized structure (as shown in Fig. 5), Molecular Docking (MD) calculations can provide valuable insights into the biological activities of molecules. It is widely acknowledged that various types of chemical interactions can contribute to the enhancement of molecular activity. Compounds with the most negative binding energy values typically exhibit the highest activity levels. The complex was tested with various bacteria including Escherichia coli, Klebsiella aerogenes, Bacillus subtilis, and Staphylococcus aureus for antibacterial study. To rationalize this testing, we have chosen one virulent protein of each bacterium and molecular docking was performed. The study shows that the complex can bind at the tight pocket of the multidrug transport protein (Fig. 7a) AcrB (1t9u) of Escherichia coli, a multidrug efflux pump, with a binding energy of − 7.27 kcal/mol. It can interact with A33, Y35, P36, T37, A39, and A299 residues of the protein by conventional, non-conventional H-bond (with NO_2 group), and hydrophobic interactions (Fig. 7b). On the protein surface of oxygen-dependent coproporphyrinogen-III oxidase (hemf) from Klebsiella aerogenes (8t7w) can also interact with the Cu-complex (Fig. 7c) and the binding energy was found to be − 5.88 kcal/mol. In this case, the nitro group and the metal-attached water molecules are involved in the H-bond with R50, Q57, M268, P269, and P270 residues of the protein. E262 residue was involved in the π…anion interactions (Fig. 7d). Again, the complex has the capability to bind with the primary wall teichoic acid ligase protein (6UF6) of Bacillus subtilis (Fig. 7e) with binding energy − 6.28 kcal/mol. Here, it prefers a surface-binding pocket and interacts with D107, D119, K120, I283, Y284, and Y285 through H-bond (nitro group and water of the complex) and π-staking interactions (Fig. 7f). The SdrD protein (4jdz) from Staphylococcus aureus is located on the cell surface as receptors to identify their ligands during infection. The compound binds at this ligand-binding site through H-bond (nitro group and water of the complex) and π-staking interactions (Fig. 7g) with K209, D307, G346, and K562 residues of the protein (Fig. 7h). Through MEP and HS analysis, we understood that the nitro group and water in the complex are poised for interactions, acting as H-bond acceptors and donors, respectively. Additionally, the aromatic rings are well-suited for π-stacking interactions. This finding was also confirmed in the docking study. Therefore, the molecule can interact with various protein molecules and inhibit their normal functions through H-bond and π-staking interactions.

Conclusion

In summary, the present article describes the synthesis, modern spectroscopic findings along with single-crystal structure analysis of one 3D-coordination polymer of copper(II) and sodium(I) $[CuNa(H\textit{hpmet})(H_2O)(OH)]_n$. EDX-SEM was utilized to examine the elemental composition and

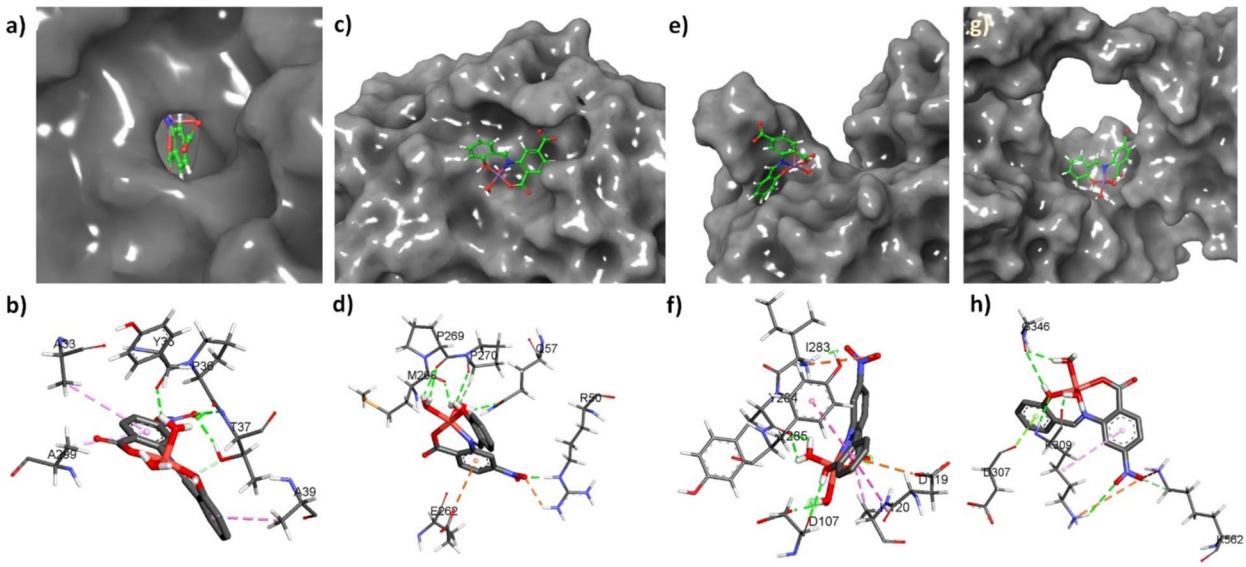

Fig. 7 Docking pose of the Cu-complex with **a** multidrug transport protein, and **b** its different non-covalent interactions with the protein; with **c** oxygen-dependent coproporphyrinogen-III oxidase (hemf) from Klebsiella aerogenes, and **d** its different non-covalent interactions with the protein; with **e** primary wall teichoic acid ligase protein, and **f** its different non-covalent interactions with the protein; with **g** SdrD protein, and **h** its different non-covalent interactions with the protein

morphological difference between the Schiff base and the complex. DFT calculations optimized the molecular geometry of the compound in gas phase. HOMO–LUMO energy gap is 2.81 V which is responsible for the high reactivity of the complex. Non-covalent interaction is present in the solid state between N–H (18.9%) and O–H (29.6%) contact and depicted from Hirshfeld surface and 2-D fingerprint plot. The complex was found to act as good antimicrobial agent with MIC value 11.25 µg/ml. In-depth in-silico molecular docking study against Gm + ve and Gm –ve bacteria's demonstrated the correlation and support the wide-range antimicrobial property of the synthesized complex. Finally, the goal of the study is that the synthesized complex may find its place as promising drug as well as antimicrobial agent.

Supplementary Information The online version contains supplementary material available at https://doi.org/10.1007/s11243-024-00621-7.

Acknowledgements S. Saha gratefully acknowledges the UGC for awarding a senior research fellowship (SRF). N. Biswas acknowledges the CSIR, New Delhi, Govt. of India, for awarding a junior research fellowship (Project No. 01/2537/11- EMR - II). M. Chowdhury acknowledges UGC, New Delhi, Government of India, for awarding senior research fellowship (Sr. No. 2121410140, ref. no. 21/12/2014 (II) EU-V). C. Roy Choudhury acknowledges the DST-FIST (Project No. SR/FST/CSI-246/2012), New Delhi, Govt. of India for instrumental support under capital heads.

Author contribution SS: conceptualization, methodology, synthesis. NB: methodology, writing—original draft preparation. MC: methodology, prepared figures. KKG: methodology. CR: software, supervision. NS: investigation, software. SC: investigation. MC: investigation, writing—original draft. CRC: writing—reviewing and editing, supervision. All authors reviewed the manuscript.

Data availability No datasets were generated or analyzed during the current study.

Declarations

Conflict of interest The authors declare no competing interests.

References

1. Nouar F, Eubank JF, Bousquet T et al (2008) Supermolecular building blocks (SBBs) for the design and synthesis of highly porous metal-organic frameworks. J Am Chem Soc 130:1833–1835. https://doi.org/10.1021/ja710123s
2. Uemura K, Saito K, Kitagawa S, Kita H (2006) Hydrogen-bonded porous coordination polymers: structural transformation, sorption properties, and particle size from kinetic studies. J Am Chem Soc 128:16122–16130. https://doi.org/10.1021/ja064152r
3. Millward AR, Yaghi OM (2005) Metal-organic frameworks with exceptionally high capacity for storage of carbon dioxide at room temperature. J Am Chem Soc 127:17998–17999. https://doi.org/10.1021/ja0570032
4. Rowsell JLC, Yaghi OM (2006) Effects of functionalization, catenation, and variation of the metal oxide and organic linking units on the low-pressure hydrogen adsorption properties of metal-organic frameworks. J Am Chem Soc 128:1304–1315. https://doi.org/10.1021/ja056639q
5. Nayak M, Koner R, Stoeckli-Evans H, Mohanta S (2005) Hydrogen-bonded one-dimensional zigzag pairs and helical dimers in an Enolic 4-Terpyridone based Nickel(II) dicyanamide supramolecule. Cryst Growth Des 5:1907–1912. https://doi.org/10.1021/cg050182e
6. Agnihotri P, Eringathodi E, Paul P et al (2006) Synthesis, crystal structures, cation-binding properties and the influence of intramolecular C–H···O interactions on the complexation behaviour of a family of cone p-tert-Butylcalix [4]arene-crown-5 compounds. Eur J Inorg Chem 17:3369–3381. https://doi.org/10.1002/ejic.200600354
7. Vogt FG, Clawson JS, Strohmeier M et al (2009) Solid-state NMR analysis of organic cocrystals and complexes. Cryst Growth Des 9:921–937. https://doi.org/10.1021/cg8007014
8. Wang WH, Xi PH, Su XY et al (2007) Supramolecular assemblies of multifunctional diimidazole and dicarboxylic acids via various hydrogen bonds and X...π (X) π, CH) interactions. Cryst Growth Des 7:741–746. https://doi.org/10.1021/cg060764b
9. Moulton B, Zaworotko MJ (2001) From molecules to crystal engineering: supramolecular isomerism and polymorphism in network solids. Chem Rev 101:1629–1658. https://doi.org/10.1021/cr9900432
10. Braga D, Maini L, Polito M et al (2001) Design of organometallic molecular and ionic materials. Coord Chem Rev 216:225–248. https://doi.org/10.1016/S0010-8545(01)00314-9
11. Thomas JA, Atwood JL, Steed JW (eds) (2004) Encyclopedia of supramolecular chemistry. CRC Press, Boca Raton, p 1248
12. Dance IG (1996) The crystals as a supramolecular entity. In: Desiraju GR (ed) The crystals as a supramolecular entity. Wiley, New York, pp 137–233
13. Sauvage JP (ed) (1999) Transition metals in supramolecular chemistry: perspectives in supramolecular chemistry, vol 5. Wiley, London
14. Jana AD, Manna SC, Rosair GM et al (2007) 4,4′-Dipyridyl-N,N′-dioxide complexes of metal-thiocyanate/selenocyanate: π-stacked molecular rods as three-dimensional support for two-dimensional polymeric sheets and intra/interchain S….S interaction dependent architecture of the R_2^2 (8) synthon driven assembly of one-dimensional polymeric chains. Cryst Growth Des 7:1365–1372. https://doi.org/10.1021/cg060762r
15. Khoo IC (2007) Liquid crystal, Wiley-Interscience. Wiley
16. Yang DK, Wu ST (2006) Fundamentals of liquid crystal devices. Wiley
17. Seddon RK, Zaworotko MJ (1999) Crystal engineering: the design and application of functional solids (NATO Science Series)
18. Desiraju GR (1989) Crystal engineering: the design of organic solids. Elsevier, Amsterdam
19. Lan H, Miao S, Zhang Y et al (2023) On the inverse correlation between the hydrogen bond strength and chalcogen bond strength in the cyclic supramolecular hetero synthon [–Se–N=]···[HOOC–]. CrystEngComm 25:2159–2164. https://doi.org/10.1039/D3CE00100H
20. Dimitrakopoulos CD, Malenfant PRL (2002) Organic thin film transistors for large area electronics. Adv Mater 14:99–117
21. Forrest SR (2004) The path to ubiquitous and low-cost organic electronic appliances on plastic. Nature 428:911–918. https://doi.org/10.1038/nature02498
22. Niu T, Jacobson AJ (1999) Syntheses and structural characterizations of the three-dimensional polymers [(R2Sn)3{Co(CN)6}2, X] (R = Vinyl, Propyl, Butyl; X =Solvent). InorgChem 38:5346–5350. https://doi.org/10.1021/ic990648g

23. Klausmeyer KK, Rauchfuss TB, Wilson SR (1998) Stepwise assembly of [(C H) (C Me) Co Rh (CN)], an "organometallic box." AngewChemInt Ed 37:1694–1696
24. Ibrahim AMA (1999) Supramolecular host–guest coordination systems: $[(G^{+})(Me_3E)_3M^{II}(CN)_6]_{\infty}$ as ion exchangers, where (G^{+}=Me_3E, Et_4N or stp), (E=Sn or Pb) and (M=Fe or Ru). Polyhedron 18:2711–2721. https://doi.org/10.1016/S0277-5387(99)00176-X
25. Meng H, Sun F, Goldfinger MB et al (2006) 2,6-Bis[2-(4-pentylphenyl)vinyl]anthracene: a stable and high charge mobility organic semiconductor with densely packed crystal structure. J Am Chem Soc 128:9304–9305. https://doi.org/10.1021/ja062683+
26. Godsell DS (2004) Bionanotechnology lessons from nature. Wiley
27. Cuyper MD, Bulte JWM (2002) Physics and chemistry basis of biotechnology. Kulwar Academic Publishers
28. Desiraju GR (1995) Supramolecular synthons in crystal engineering—a new organic synthesis. Angew Chem Int Ed Engl 34:2311–2327. https://doi.org/10.1002/anie.199523111
29. Saha S, Choudhury CR, Gómez-García C et al (2017) Magneto-structural and theoretical study of the weak interactions in a Mn(II) complex with a very unusual N, O-chelating coordination mode of 2-aminoterephthalate. Inorg Chim Acta 461:183–191. https://doi.org/10.1016/j.ica.2017.02.016
30. Ghosh AK, Jana AD, Ghoshal D et al (2006) Toward the recognition of enolates/dicarboxylates: syntheses and X-ray crystal structures of supramolecular architectures of Zn(II)/Cd(II) Using 2,2'-Biimidazole. Cryst Growth Des 6:701–707. https://doi.org/10.1021/cg050473n
31. Janiak CJ (2000) A critical account on π–π stacking in metal complexes with aromatic nitrogen-containing ligands. Chem Soc Dalton Trans 21:3885–3896. https://doi.org/10.1039/B003010O
32. Sinnokrot MO, Sherrill CD (2006) High-accuracy quantum mechanical studies of π–π interactions in benzene dimers. J Phys Chem A 110:10656–10668. https://doi.org/10.1021/jp0610416
33. Lee EC, Kim D, Jurecka P et al (2007) Understanding of assembly phenomena by aromatic–aromatic interactions: benzene dimer and the substituted systems. J Phys Chem 111:3446–3457. https://doi.org/10.1021/jp068635t
34. Pitonak M, Neogrady P, Rezac J et al (2008) Benzene dimer: high-level wave function and density functional theory calculations. J Chem Theory Comput 4:1829–1834. https://doi.org/10.1021/ct800229h
35. Singh NJ, Min SK, Kim DY et al (2009) Comprehensive energy analysis for various types of π-interaction. J Chem Theory Comput 5:515–529. https://doi.org/10.1021/ct800471b
36. Mayer EA, Castellano RK, Diederich F (2003) Interactions with aromatic rings in chemical and biological recognition. Angew Chem Int Ed 42:1210–1250. https://doi.org/10.1002/anie.200390319
37. Nishio M, Hirota M, Umezawa Y (1998) The C–H···π interaction: evidence, nature and consequences. Wiley-VCH, New York
38. Nishio M (2004) CH/p hydrogen bonds in crystals. CrystEngComm 6:130–158. https://doi.org/10.1039/B313104A
39. Fernandez-Alonso MDC, Canada FJ, Jimenez-Barbero J et al (2005) Molecular recognition of saccharides by proteins. Insights on the origin of the carbohydrate–aromatic interactions. J Am Chem Soc 127:7379–7386. https://doi.org/10.1021/ja051020+
40. Owen SM (1988) Electron counting in clusters: a view of the concepts. Polyhedron 7:253–283. https://doi.org/10.1016/S0277-5387(00)80467-2
41. Mingos DMP (1972) A general theory for cluster and ring compounds of the main group and transition elements. Nat Phys Sci (London) 236:99–102. https://doi.org/10.1038/physci236099a0
42. Wade K (1976) Structural and bonding patterns in cluster chemistry. Adv Inorg Chem Radio Chem 18:1–66. https://doi.org/10.1016/S0065-2792(08)60027-8
43. Mingos DMP, Watson MJ (1992) Heteronuclear gold cluster compounds. Adv Inorg Chem 39:327–399. https://doi.org/10.1016/S0898-8838(08)60262-7
44. Reynolds RA, Coucouvanis D (1988) Mixed carboxylate/catecholate polynuclear complexes. Integral association of trivalent lanthanide ions with Mn4 units in the pentanuclear Mn4LaCl and Mn4Tb clusters. J Am Chem Soc 120:209–210. https://doi.org/10.1021/ja971451v
45. Murrie M, Parsons S, Winpenny REP (1998) Deltahedra as underlying structural motifs in polynuclear metal chemistry: structure of an undecanuclear manganese–potassium cage. J Chem Soc Dalton Trans 9:1423–1424. https://doi.org/10.1039/A800829I
46. Brechin EK, Graham A, Harris SG et al (1997) Overcrowding leads to prism reform: new polyhedra for polymetallic cages. J Chem Soc Dalton Trans 19:3405–3406. https://doi.org/10.1039/A704822J
47. Muller A, Peters F, Pope MT et al (1998) Polyoxometalates: very large clusters nanoscale magnets. Chem Rev 98:239–272. https://doi.org/10.1021/cr9603946
48. Zhang Y, Zapf PJ, Meyer LM et al (1997) Polyoxoanion coordination chemistry: synthesis and characterization of the heterometallic, hexanuclear clusters [{Zn(bipy)2}2V4O12], [{Zn(phen)2}2V4O12], H2O, and [{Ni(bipy)2}2Mo4O14]. Inorg Chem 36:2159–2165. https://doi.org/10.1021/ic961045x
49. Suber L, Bonamico M, Fares V (1997) Synthesis, magnetism, and X-ray molecular structure of the mixed-valence vanadium (IV/V)-oxygen cluster $[VO4\subset(V18O45)]^{9-}$. Inorg Chem 36:2030–2033. https://doi.org/10.1021/IC960706N
50. Jeon YM, Kim J, Whang D et al (1996) Molecular container assembly capable of controlling binding and release of its guest molecules: reversible encapsulation of organic molecules in sodium ion complexed cucurbituril. J Am Chem Soc 118:9790–9791. https://doi.org/10.1021/ja962071x
51. Piotrowski H, Polborn K, Hilt G et al (2001) A self-assembled metallomacrocyclic ionophore with high affinity and selectivity for Li^{+} and Na^{+}. J Am Chem Soc 123:2699–2700. https://doi.org/10.1021/ja005804t
52. Abrahams BF, FitzGerald NJ, Hudson TA et al (2007) Aust J Chem 60:68–71
53. Thakurta S, Chakraborty J, Rosair G et al (2008) Synthesis of two new linear trinuclear Cu^{II} complexes: mechanism of magnetic coupling through hybrid B3LYP functional and CShM studies. Inorg Chem 47:6227–6235. https://doi.org/10.1021/ic8001459
54. Agapiou K, Mejia ML, Yang X et al (2009) Multinuclear Cd2, Cd3 and 1-D framework structures of Cd(II) Schiff base complexes. Dalton Trans 21:4154–4159. https://doi.org/10.1039/B816059G
55. Bhowmik P, Chatterjee S, Chattopadhyay S (2013) Heterometallic inorganic–organic frameworks of sodium–nickel (vanen): Cation–π interaction, trigonal dodecahedral Na^{+} and unprecedented heptadentate coordination mode of $vanen^{2-}$. Polyhedron 63:214–221. https://doi.org/10.1016/j.poly.2013.07.023
56. Bhowmik P, Jana S, Jana PP et al (2012) Unique example of a T3(2)4(2)3(2)6(2) water tape containing acetate–water hybrid hexamer in a heterometallicschiff base complex host. Inorg Chem Commun 18:50–56. https://doi.org/10.1016/j.inoche.2012.01.008
57. Mahlooji N, Behzad M, Rudbari HA et al (2016) Unique examples of copper(II)/sodium(I) and nickel(II)/sodium(I) Schiff base complexes with bridging bis-bidentate Salen type ligand: synthesis, crystal structures and antibacterial studies. Inorg Chim Acta 445:124–128. https://doi.org/10.1016/j.ica.2016.02.040

58. Das M, Chatterjee S, Chattopadhyay S (2011) Unique example of a trigonal dodecahedral Na^+ in a compartmental Schiff base N, N′-(1,2-Phenylene)-bis(3-methoxysalicylideneimine). Inorg Chem Commun 14:1337–1340. https://doi.org/10.1016/j.inoche.2011.05.009
59. Sasmal A, Saha S, Gómez-García C et al (2013) Reversible switching of the electronic ground state in a penta coordinated Cu(II) complex. Chem Commun 49:7806–7808. https://doi.org/10.1039/C3CC44276D
60. Iranmanesh H, Behzad M, Bruno G et al (2013) Cobalt(III) Schiff base complexes derived from mesostilbenediamine: synthesis, characterization, crystal structure, electrochemistry and antibacterial studies. Inorg Chim Acta 395:81–88. https://doi.org/10.1016/j.ica.2012.10.030
61. Majumdar D, Frontera A, Roy S et al (2023) Experimental and theoretical survey of intramolecular spodium bonds/σ/π-holes and noncovalent interactions in trinuclear Zn(II)- salen type complex with OCN^- ions: a holistic view in crystal engineering. ACS Omega 9:1786–1797. https://doi.org/10.1021/acsomega.3c08422
62. Majumdar D, Gassoumi B, Dey A et al (2024) Synthesis, characterization, crystal structure, and fabrication of photosensitive Schottky device of a binuclear Cu(II)-Salen complex: a DFT investigations. RSC Adv 14:14992–15007. https://doi.org/10.1039/d4ra01846j
63. Saha S, Biswas N, Sasmal A et al (2018) Effect of temperature and ligand protonation on the electronic ground state in Cu(II) polymers having unusual secondary interactions: a magnetic and catechol oxidase study. Dalton Trans 47:16102–16118. https://doi.org/10.1039/C8DT02417K
64. Majumdar D, Roy S, Philip JS, Tüzün B, Hazra S et al (2024) In-situ Salen-type ligand formation-driven of a heterometallic Cu(II)–Hg(II) complex: synthetic update, crystallographic features, DFT calculations, and unveil antimicrobial profiles. Inorg Chem Commun 160:111933. https://doi.org/10.1016/j.inoche.2023.111933
65. Gheorghe R, Cucos P, Andruh M et al (2006) Oligonuclear 3d–4f complexes as tectons in designing supramolecular solid-state architectures: impact of the nature of linkers on the structural diversity. Chem Eur J 12:187–203. https://doi.org/10.1002/chem.200500321
66. Visinescu D, Madalan AM, Andruh M et al (2009) First heterotrimetallic 3 d-4 d-4 f single chain magnet, constructed from anisotropic high-spin heterometallic nodes and paramagnetic spacers. Chem Eur J 15:11808–11814. https://doi.org/10.1002/chem.200902408
67. Franceschi F, Solari E, Floriani C, Rosi M, Chiesi-Villa A, Rizzoli C (1999) Chem Eur J 5:708–721
68. Chakrabarty PP, Biswas D, García-Granda S et al (2012) Sodium ion assisted molecular self-assembly in a class of Schiff-base copper(II) complexes. Polyhedron 35:108–115. https://doi.org/10.1016/j.poly.2012.01.004
69. Vigato PA, Tamburini S (2004) The challenge of cyclic and acyclic schiff bases and related derivatives. Coord Chem Rev 248:1717–2128. https://doi.org/10.1016/j.cct.2003.09.003
70. Saha S, Sasmal A, Choudhury CR et al (2015) Synthesis, crystal structure, antimicrobial screening and density functional theory calculation of nickel(II), cobalt(II) and zinc(II) mononuclear Schiff base complexes. Inorg Chim Acta 425:211–220. https://doi.org/10.1016/j.ica.2014.10.007
71. APEX2, SADABS, SMART and SAINT (2008) Bruker AXS Inc., Madison, WI, USA, 2000
72. Altomare A, Burla MC, Camalli M et al (1999) SIR97: a new tool for crystal structure determination and refinement. J Appl Crystallogr 32:115–119. https://doi.org/10.1107/S0021889898007717
73. Sheldrick GM (2015) Crystal structure refinement with SHELXL. Acta Crystallogr C71:3–8. https://doi.org/10.1107/S2053229614024218
74. Watkin DJ, Prout CK, Pearce LJ (1996) CAMERON. Chemical Crystallography Laboratory, University of Oxford, Oxford
75. Spek AL (1990) PLATON, an integrated tool for the analysis of the results of a single crystal structure determination. Acta Crystallogr 46:C34. https://doi.org/10.1107/S0108767390099780
76. Brandenburg K, Brandenburg K, Putz H, Brandenburg K and Berndt M (1999) DIAMOND, Crystal Impact GbR, Bonn, Germany
77. Persistence of Vision Pty. Ltd. (2004) Persistence of vision raytracer (Version 3.6), Computer Software, Retrived from http://www.povray.org/download/
78. Dolomanov OV, Bourhis LJ, Gildea RJ et al (2009) OLEX2: a complete structure solution, refinement and analysis program. J Appl Cryst 42:339–341. https://doi.org/10.1107/S0021889808042726
79. Spackman MA, Jayatilaka D (2009) Hirshfeld surface analysis. CrystEngComm 11:19–32. https://doi.org/10.1039/B818330A
80. Wolff SK, Grimwood DJ, McKinnon JJ, Turner MJ, Jayatilaka DMA and Spackman MA (2012) Crystal Explorer 3.1. University of Western Australia
81. Sepay N, Banerjee M, Islam R et al (2022) Crystallography-based exploration of non-covalent interactions for the design and synthesis of coumarin for stronger protein binding. Phys Chem Chem Phys 24:6605–6615. https://doi.org/10.1039/D2CP00082B
82. Sepay N, Saha PC, Shahzadi Z et al (2021) A crystallography-based investigation of weak interactions for drug design against COVID-19. Phys Chem Chem Phys 23:7261–7270. https://doi.org/10.1039/D0CP05714B
83. Seth SK, Sarkar D, Roy A et al (2011) Insight into supramolecular self-assembly directed by weak interactions in acetophenone derivatives: crystal structures and Hirshfeld surface analyses. CrystEngComm 13:6728–6741. https://doi.org/10.1039/C1CE05670K
84. Gaussian 09, Revision D.01; Gaussian, Inc.: Wallingford, CT, Gaussian 09, Revision D.01; Gaussian, Inc.: Wallingford, CT, 2009
85. GaussView, Gaussian, Inc., (2009)
86. Blatov VA, Shevchenko AP, Proserpio DM (2014) Applied topological analysis of crystal structures with the program package ToposPro. Cryst Growth Des 14:3576–3586. https://doi.org/10.1021/cg500498k
87. O'Keeffe M, Peskov MA, Ramsden SJ et al (2008) The reticular chemistry structure resource (RCSR) database of, and symbols for, crystal nets. Acc Chem Res 41:1782–1789. https://doi.org/10.1021/ar800124u
88. Alexandrov EV, Blatov VA, Kochetkov AV et al (2011) Underlying nets in three-periodic coordination polymers: topology, taxonomy and prediction from a computer-aided analysis of the Cambridge Structural Database. CrystEngComm 13(3947):3958. https://doi.org/10.1039/C0CE00636J
89. Milburn H, Truter MR, Vickery BL (1974) Crystal structure of a sodium complex, bis-[NN′-ethylenebis(salicylideneiminato) copper(II)]perchloratosodium–p-xylene. J Chem Soc Dalton Trans 1974:841–846. https://doi.org/10.1039/DT9740000841
90. Saha PK, Dutta B, Jana S et al (2007) Immobilization of a copper-Schiff base complex in a Y-zeolite matrix: preparation, chromogenic behavior and catalytic oxidation. Polyhedron 26:563–571. https://doi.org/10.1016/j.poly.2006.08.018
91. Bhowmik P, Harms K, Chattopadhyay S et al (2013) Formation of polynuclear copper(II)–sodium(I) heterometallic complexes derived from salen-type Schiff bases. Polyhedron 49:113–120. https://doi.org/10.1016/j.poly.2012.09.058

92. Biswas D, Chakrabarty PP, Saha S et al (2013) Ligand mediated structural diversity and role of different weak interactions in molecular self-assembly of a series of copper(II)–sodium(I) Schiff-baseheterometallic complexes. Inorg Chim Acta 408:172–180. https://doi.org/10.1016/j.ica.2013.09.011
93. Mukherjee P, Drew MGB, Figuerola A et al (2008) Incorporation of a sodium ion guest in the host of copper(II)-Schiff-base complexes: structural characterization and magnetic study. Polyhedron 27:3343–3350. https://doi.org/10.1016/j.poly.2008.07.025
94. Biswas N, Khanra S, Sarkar A et al (2017) One new azido bridged dinuclearcopper(II) thiosemicarbazide complex: synthesis, DNA/protein binding, molecular docking study and cytotoxicity activity. New J Chem 41:12996–13011. https://doi.org/10.1039/C7NJ01998J
95. Das K, Datta A, Roy S et al (2014) Doubly phenoxo-bridged M–Na (M = Cu(II), Ni(II)) complexes of tetradentate Schiff base: structure, photoluminescence, EPR, electrochemical studies and DFT computation. Polyhedron 78:62–71. https://doi.org/10.1016/j.poly.2014.04.032
96. Das M, Mukherjee S, Koley B et al (2020) Developing novel zinc(II) and copper(II) Schiff base complexes: combined experimental and theoretical investigation on their DNA/protein binding efficacy and anticancer activity. New J Chem 44:18347–18361. https://doi.org/10.1039/D0NJ03844J
97. Nakamoto K (2009) Infrared and Raman spectra of inorganic and coordination compounds. Part B: Applications in coordination, organometallic, and bioinorganic chemistry, 5th ed, p 64. Wiley, New York
98. Shebl M, Khalil SME, Ahmed SA et al (2010) Synthesis, spectroscopic characterization and antimicrobial activity of mono-, bi- and tri-nuclear metal complexes of a new Schiff base ligand. J Mol Struct 980:39–50. https://doi.org/10.1016/j.molstruc.2010.06.034
99. Hassanien MM, Gabr IM, Abdel-Rhman MH et al (2008) Synthesis and structural investigation of mono- and polynuclear copper complexes of 4-ethyl-1-(pyridin-2-yl) thiosemicarbazide. Spectrochim Acta A Mol Biomol Spectrosc 71:73–79. https://doi.org/10.1016/j.saa.2007.11.009
100. Biswas BK, Saha S, Biswas N et al (2020) Two copper (II) complexes derived from anthranilic acid and 4-iodo-anthranilic acid Schiff bases: Structural elucidation, halogen bonding interactions and catalytic study using 3,5-DTBC. J Mol Struct 1217:128398–128412. https://doi.org/10.1016/j.molstruc.2020.128398
101. Lever ABP (1984) Inorganic electronic spectroscopy, 2nd edn. Elsevier, Amsterdam
102. Biswas N, Khanra S, Sarkar A et al (2018) Cytotoxicity activity, in silico molecular docking, protein- and DNA-binding study of a new Ni(II) Schiff base complex. J Coord Chem 71:2740–2766. https://doi.org/10.1080/00958972.2018.1492118
103. Addison AW, Rao TN, Reedijk J et al (1984) Synthesis, structure, and spectroscopic properties of copper(II) compounds containing nitrogen–sulphur donor ligands; the crystal and molecular structure of aqua[1,7-bis(N-methylbenzimidazol-2′-yl)-2,6-dithiaheptane]copper(II) perchlorate. J Chem Soc Dalton Trans 7:1349–1356. https://doi.org/10.1039/DT9840001349
104. Tweedy BG (1964) Plant extracts with metal ions as potential antimicrobial agents. Phytopathology 55:910–918
105. Nain-Perez A, Barbosa LCA, Araujo MH et al (2021) Antibacterial and cytotoxic activity of ruthenium-p-cymene complexes with 2-Methylquinolin-8-ol derivatives. Chem Sel 6:2942–2950. https://doi.org/10.1002/slct.202100733
106. Majumdar D, Philip JE, Gassoumi B et al (2024) Supramolecular clumps of μ2-1,3-acetate bridges of Cd(II)-Salen complex: synthesis, spectroscopic characterization, crystal structure, DFT quantization's, and antifungal photodynamic therapy. Heliyon 10:E29856. https://doi.org/10.1016/j.heliyon.2024.e29856
107. Klaimanee E, Nhukeaw T, Saithong S et al (2021) Half-sandwich ruthenium (II) p-cymene complexes based on organophosphorus ligands: Structure determination, computational investigation, in vitro antiproliferative effect in breast cancer cells and antimicrobial activity. Polyhedron 204:115244–115254. https://doi.org/10.1016/j.poly.2021.115244
108. Namiecinska E, Grazul M, Sadowska B et al (2022) Arene-Ruthenium(II) complexes with carbothiamidopyrazoles as a potential alternative for antibiotic resistance in human. Molecules 27:468–491. https://doi.org/10.3390/molecules27020468

Publisher's Note Springer Nature remains neutral with regard to jurisdictional claims in published maps and institutional affiliations.